‖‖ 1.0

2.8   2.5

3.2   2.2

3.6

4.0   2.0

‖ 1.1

1.8

‖ 1.25   1.4   1.6

MICROCOPY RESOLUTION TEST CHART

NATIONAL BUREAU OF STANDARDS 1963 A

LEVEL

ALGORITHM INVESTIGATION FOR LARGE ADAPTIVE ARRAYS

Stanford University

B. Widrow   R. Gooch
H. Mesiwala   F. McCarthy
K. Duvall   W. Newman
P. Titchener

AD A089753

DTIC
ELECTE
SEP 3 0 1980
C

ROME AIR DEVELOPMENT CENTER
Air Force Systems Command
Griffiss Air Force Base, New York 13441

DDC FILE COPY

80 9 30 012

This report has been reviewed by the RADC Public Affairs Office (PA) and is releasable to the National Technical Information Service (NTIS). At NTIS it will be releasable to the general public, including foreign nations.

RADC-TR-80-234 has been reviewed and is approved for publication.

APPROVED: *John A. Graniero*

JOHN A. GRANIERO
Project Engineer

APPROVED: *Fred I. Diamond*

FRED I. DIAMOND, Technical Director
Communications and Control Division

FOR THE COMMANDER: *John P. Huss*

JOHN P. HUSS
Acting Chief, Plans Office

SUBJECT TO EXPORT CONTROL LAWS

This document contains information for manufacturing or using munitions of war. Export of the information contained herein, or release to foreign nationals within the United States, without first obtaining an export license, is a violation of the International Traffic in Arms Regulations. Such violation is subject to a penalty of up to 2 years imprisonment and a fine of $100,000 under 22 U.S.C 2778.

Include this notice with any reproduced portion of this document.

If your address has changed or if you wish to be removed from the RADC mailing list, or if the addressee is no longer employed by your organization, please notify RADC.(DCCR) Griffiss AFB NY 13441. This will assist us in maintaining a current mailing list.

Do not return this copy. Retain or destroy.

UNCLASSIFIED

REPORT DOCUMENTATION PAGE	READ INSTRUCTIONS BEFORE COMPLETING FORM

1. REPORT NUMBER	2. GOVT ACCESSION NO.	3. RECIPIENT'S CATALOG NUMBER
RADC-TR-80-234	AD-A089 753	

4. TITLE (and Subtitle)	5. TYPE OF REPORT & PERIOD COVERED
ALGORITHM INVESTIGATION FOR LARGE ADAPTIVE ARRAYS	Final Technical Report 15 May 78 — 31 Dec 79
	6. PERFORMING ORG. REPORT NUMBER N/A

7. AUTHOR(s)	8. CONTRACT OR GRANT NUMBER(s)
B. Widrow P. Titchener W. Newman H. Mesiwala R. Gooch K. Duvall F. McCarthy	F30602-78-C-0083 N00019-79-C-0331

9. PERFORMING ORGANIZATION NAME AND ADDRESS	10. PROGRAM ELEMENT, PROJECT, TASK AREA & WORK UNIT NUMBERS
Stanford University Stanford CA 94305	61102F 23050823 58

11. CONTROLLING OFFICE NAME AND ADDRESS	12. REPORT DATE
Rome Air Development Center (DCCR) Griffiss AFB NY 13441	July 1980
	13. NUMBER OF PAGES 72

14. MONITORING AGENCY NAME & ADDRESS(if different from Controlling Office)	15. SECURITY CLASS. (of this report)
Same	UNCLASSIFIED
	15a. DECLASSIFICATION/DOWNGRADING SCHEDULE N/A

16. DISTRIBUTION STATEMENT (of this Report)

Approved for public release; distribution unlimited.

17. DISTRIBUTION STATEMENT (of the abstract entered in Block 20, if different from Report)

Same

18. SUPPLEMENTARY NOTES

RADC Project Engineer: John Graniero (DCCR)

19. KEY WORDS (Continue on reverse side if necessary and identify by block number)
Adaptive Antenna
Adaptive Arrays
Adaptive Filters
LMS Algorithm
Null Steering

20. ABSTRACT (Continue on reverse side if necessary and identify by block number)

This report examines the influence of surplus antenna elements in an adaptive array. It is demonstrated that the judicious placement of a few extra antenna elements provides significant performance improvement. In particular, the speed of convergence is improved, and the quality of the antenna beam pattern is enhanced.

(Continued)

DD FORM 1473 EDITION OF 1 NOV 65 IS OBSOLETE

UNCLASSIFIED

Item 20 (Continued)

Convergence rates and beam patterns are closely related to the eigenvalues of the antenna/signal system. A closed form expression is derived for the eigenvalues of a general antenna array with two jammers. From this, expressions for the convergence rate and the optimum beam pattern are found. Computer simulations are used to verify the theoretical developments concerning convergence rates and final beam patterns for a variety of element configurations.

ACKNOWLEDGMENT

Accession For

NTIS GRA&I	✓	
DDC TAB	☐	
Unannounced	☐	
Justification		

By

Distribution/

Availability Codes

Dist	Avail and/or special
A	

1

EVALUATION

This effort is a part of Research Area 7, Electronics, Sub-Area 3, Communications. The objective is to investigate the convergence properties of adaptive algorithms for arrays with a large number of antenna elements or weights. This research work supports RADC TPO Sub-Thrust 4B1, Adaptive Processing for Communications. The overall objective of this sub-thrust is to advance the state-of-the-art in adaptive spatial processing to provide an Electronic Counter Counter-measure (ECCM) capability for Air Force Communications Systems.

In this research effort, it was demonstrated that the judicious placement of a few extra antenna elements provides significant performance improvement. It was also shown that convergence rates and beam patterns are closely related to the eigenvalues of the antenna/ signal system. A closed form expression was derived for the eigenvalues of a general antenna array with two jammers. From this expression, the estimated convergence rate and the optimum beam pattern are found for particular antenna array geometries.

This is a significant step in providing the analytical expressions enabling selecting the optimum antenna array geometry for convergence and beam pattern shape given bounds on overall physical array dimensions and numbers of antenna elements.

JOHN A. GRANIERO
Project Engineer

I.   INTRODUCTION

Adaptive antenna array systems can be used to steer nulls in the direction of arrival of interfering signal sources (jammers).[1] Previous analyses and simulations relating to these adaptive null steerers have focused attention on the nulling of a single jammer or of multiple jammers with equal power and wide angular separation.[2,3,4]

When two or more jammers with widely differing power levels are involved, the time required to null all jammers can become very long in comparison with the time required to null a single jammer. This problem has been pointed out by White[5] and Reed *et al.*[6] Furthermore, the antenna pattern at convergence may fail to exhibit the sharp nulls that are needed to eliminate interference with minimal impact on desired signals.

The purpose of the research reported in this paper is twofold. First, the impact of surplus elements on convergence rate is explored. Analyses and computer simulations are presented to demonstrate the effectiveness of adding extra antenna elements to the adaptive null steerer (ANS) in order to speed up the adaptive nulling process for two closely spaced jammers with disparate power levels. Second, the effect of surplus elements on the converged beam pattern is considered. A closed form expression for the optimal beam pattern is used to directly compute the converged beam pattern. This closed form expression provides confirmation of the simulation results and furnishes a computationally efficient means of exploring the converged beam patterns for different element configurations.

3

II. DEMONSTRATION OF THE PROBLEM

A. Rate of Convergence

To demonstrate the slowness in the nulling process, a minimal adaptive sidelobe canceller structure (Fig. 2-1) having one primary element and two auxiliary elements is employed to null two jammers, designated as follows:

J_1 = Jammer 1 with power 100, incident at $40°$, frequency = 0.231/T

J_2 = Jammer 2 with power 1, incident at $55°$, frequency = 0.170/T

T = sampling period .

The array elements are spaced a quarter wavelength apart at the frequency of 0.2/T. The angular position of J_1 is chosen rather arbitrarily, while that of J_2 is chosen reasonably close to J_1. The desired signal, not explicitly included in this simulation, was assumed to be of much lower power level than that of either jammer. No constraints were used in this system to prevent cancellation of the desired signal. The intent is to obtain a beam pattern of unit gain in all directions except where high power jammers are incident. There, the gain should be very small indeed.

To focus attention on the essence of the problem it is assumed that the jammers are narrowband signals which may be approximated by sinusoids. Thus $90°$ phase shifters (instead of tapped delay lines) are used on each auxiliary antenna element. The LMS adaptive algorithm[7] is used in a simulation involving the configuration of Fig. 2-1. After a few adaptations the weights are frozen and the resulting antenna beam pattern[‡] is plotted. Then the adaptive process is resumed and the

---

[‡]The beam pattern is the array response to a unit power test signal which is swept over $360°$ while keeping the adjustable weights frozen.

J_2 @ 55^0, $P_2 = 1$, $f_2 = .170/T$

J_1 @ 40^0, $P_1 = 100$, $f_1 = .231/T$

.25υ

.25υ

Auxiliary Element

Auxiliary Element

-90

-90

Error Signal

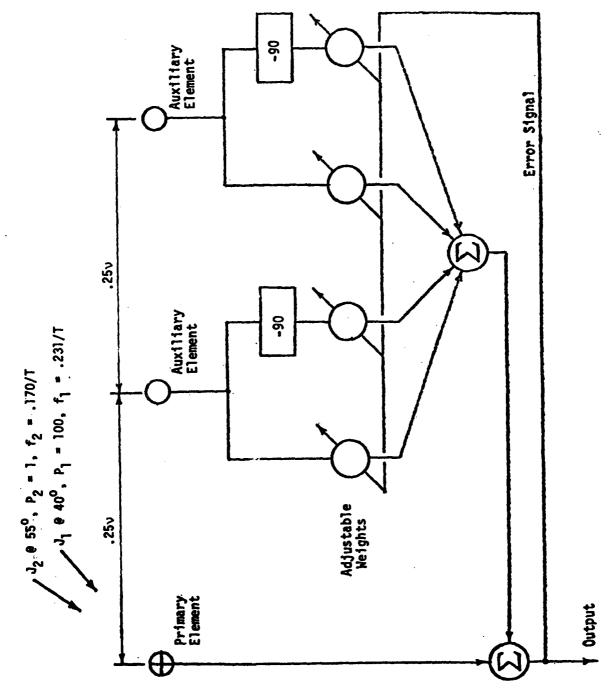Adjustable Weights

Primary Element

Output

Figure 2-1. Linear Array with Two Auxiliary Elements.

pattern plotting procedure is repeated at frequent intervals. It may be noted that no noise is added to the signals in order to concentrate exclusively on the convergence problems due to the jamming signals.
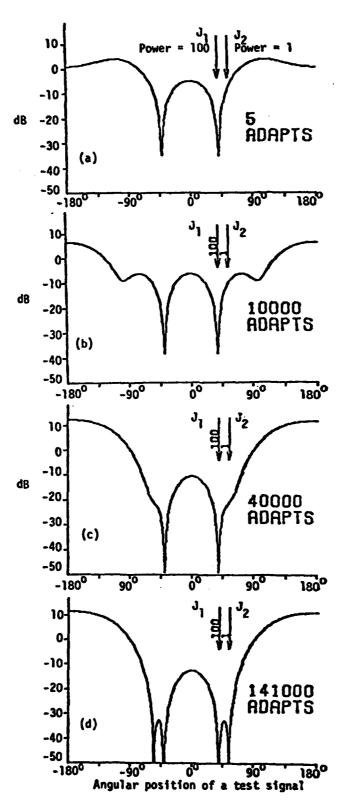
Figures 2-2a through 2-2d show a time sequence of beam patterns achieved by the above simulation as adaptation proceeds. The arrows in the figure indicate the positions of the jammers.

From Fig. 2-2a it is clear that the high-power jammer is nulled quickly, but the low-power jammer is essentially unaffected at the outset. In Fig. 2-2b the pattern has changed substantially; but it still shows little nulling effect in the area of the low-power jammer. After about 40,000 adapts the low-power signal begins to be nulled as shown in Fig. 2-2c. Well formed nulls begin to occur after about 70,000 adapts. Good nulls are achieved by about 120,000 adapts. For the purpose of this paper, convergence may be defined as the minimum number of adapts needed to reduce the output power to below 1×10^{-6}. For the configuration in Fig. 2-1, this occurs around 141,000 iterations. The converged pattern is shown in Fig. 2-2d. If the sampling rate were 1 MHz, 141,000 adapts would require 0.141 sec.

The sluggishness of the adaptive process in nulling the low-power jammer may be explained with the aid of the analysis presented in section III.

B. Final Pattern Characteristics

The converged beam pattern (Fig. 2-2d) of the minimal system is symmetric about 0° because a line array of antenna elements is unable to distinguish between positive and negative angles of arrival. The additional nulls introduced by symmetry are undesired since they may be

NOTE: Beam patterns plotted for f = .2/T

Fig. 2-2. A time sequence of beam patterns
for the ANS of Fig. 2-1.

7

in the direction of the desired signal. The broadness of the nulls also may cause attenuation of any signal with an angular location that is close to that of either of the symmetric nulls. A desirable pattern would be omnidirectional with sharp nulls in only the directions of the jammers.

The improvements in the final pattern due to restructuring of the antenna array will be detailed in section VII.

III. ANALYSIS RELATING TO CONVERGENCE RATE OF ADAPTIVE ARRAYS

A generalized version of the adaptive antenna array of Fig. 2-1 is shown in Fig. 3-1. The kth auxiliary element is located at a distance ℓ_k (given in units of wavelengths) from the primary element at an angle α_k with an arbitrary reference axis. Two jammers (J_1 and J_2) with powers ρ_1 and ρ_2 (at each antenna element) arrive at angles ψ_1 and ψ_2 as shown in the figure.

Central to the analysis of the adaptive linear combiner of the type used in Fig. 3-1 is the correlation matrix R (Widrow *et al*)[7] defined by

$$R \triangleq E(X_i, X_j) \qquad (3-1)$$

where $E(X_i, X_j)$ is the statistical correlation between the signals X_i and X_j where i, j = 1, 2, ..., 2n. The speed of convergence is intimately related to the eigenvalues of R, as can be seen from the following.

For stability of the LMS adaptive algorithm [see (24) of Widrow[7]] the adaptation constant μ must satisfy

$$1/\lambda_{max} > \mu > 0 \qquad (3-2a)$$

where λ_{max} is defined as the maximum eigenvalue of the R matrix. Maximum speed is obtained with

$$\mu = 1/2\lambda_{max} \ . \qquad (3-2b)$$

The dynamics of the adaptive system depend only on the nonzero eigenvalues of R. For every nonzero eigenvalue λ_i, the time constant τ_i of the corresponding mode is given by [see (27) of Widrow[7]]
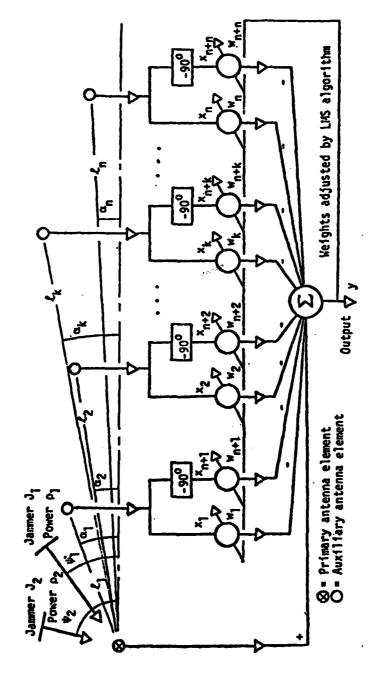
9

Fig. 3-1. An Adaptive Null Steerer with one primary and n auxiliary antenna elements.

⊗ = Primary antenna element
○ = Auxiliary antenna element

10

$$\tau_i = 1/2\mu\lambda_i \quad . \tag{3-3}$$

(τ_i is dimensionless. It is expressed in number of adapts.)

The rate of convergence with a specified μ is thus bounded above by the minimum <u>nonzero</u> eigenvalue λ_{min}. From (3-3):

$$\tau_{max} = 1/2\mu\lambda_{min} \quad . \tag{3-4}$$

Using relation (3-2b), when adapting at the maximum rate consistent with the requirements for stability, the time constant of the slowest mode will be

$$\tau_{max} = \lambda_{max}/\lambda_{min} \quad . \tag{3-5}$$

In practice the μ is required to be small compared with $1/\lambda_{max}$ to keep the misadjustment[†] within an acceptable limit. Therefore τ_{max} is greater than that indicated by equation (3-5). Nevertheless, the ratio $\lambda_{max}/\lambda_{min}$ in the right hand side (RHS) of (3-5) is a useful measure for comparing speeds of convergence, as will be seen from the examples discussed in sections IV and V.

From a detailed analysis given in Appendix A, it is shown that the eigenvalues for the general case in Fig. 3-1 take on the values given by the following expressions:

[†]Using the definition from Reference 7:

$$\text{Misadjustment} \triangleq M = \frac{\text{Average excess mean squared error (mse)}}{\text{mse obtained with optimum weight setting}}$$

$$\lambda_1 = \frac{n}{2}(\rho_1 + \rho_2) + \left[\frac{n^2}{4}(\rho_1 - \rho_2)^2 + \rho_2\rho_1 |U_1^* U_2|^2\right]$$

$$\lambda_2 = \frac{n}{2}(\rho_1 + \rho_2) - \left[\frac{n^2}{4}(\rho_1 - \rho_2)^2 + \rho_2\rho_1 |U_1^* U_2|^2\right]$$

$$\lambda_{n+1} = \lambda_1 ; \quad \lambda_{n+2} = \lambda_2$$

$$\lambda_m = 0 \quad \text{for} \quad m \notin \{1, 2, n+1, n+2\}$$

where

$$U_j \triangleq \left[e^{-i\phi_{1j}}, e^{-i\phi_{2j}}, \ldots, e^{-i\phi_{nj}}\right]^T$$

(3-6)

$$j = 1, 2 \text{ (jammer index)}$$

$U_1^* \triangleq$ Complex conjugate transpose of U_1

$$\phi_{kj} \triangleq 2\pi\ell_k \cos(\psi_j - \alpha_k)$$

$k = 1, \ldots, n$ (auxiliary element index)

$\ell_k \triangleq$ distance of kth antenna element from the primary antenna element (ℓ_k given in units of wave length)

$\alpha_k =$ Angle of kth element with respect to the reference axis (see Fig. 3).

$\psi_i =$ Angle of ith jammer

$\rho_i =$ Power of ith jammer

The ratio of maximum eigenvalue to minimum nonzero eigenvalue is thus given by

$$\frac{\lambda_{max}}{\lambda_{min}} = \frac{\lambda_1}{\lambda_2}$$

$$= \frac{\dfrac{(\rho_1+\rho_2)}{2} + \left[\dfrac{(\rho_1-\rho_2)^2}{4} + \rho_1\rho_2 \dfrac{|U_1^* U_2|^2}{n^2}\right]^{\frac{1}{2}}}{\dfrac{(\rho_1+\rho_2)}{2} - \left[\dfrac{(\rho_1-\rho_2)^2}{4} + \rho_1\rho_2 \dfrac{|U_1^* U_2|^2}{n^2}\right]^{\frac{1}{2}}} \quad . \qquad (3\text{-}7)$$

From the definition of U_j in (3-6) it is seen that $|U_1^* U_2|$ varies between 0 and n. Thus for given ρ_1 and ρ_2 ($\rho_1 \geq \rho_2$), the ratio $\lambda_{max}/\lambda_{min}$ varies between ρ_1/ρ_2 and ∞. $\lambda_{max}/\lambda_{min}$ must be kept small in order to keep τ_{max} small [see (3-5)]. Therefore the number of elements and their geometrical arrangement in the array are to be chosen such that the ratio $\lambda_{max}/\lambda_{min}$ is kept near ρ_1/ρ_2 for most ψ_1 and ψ_2 of practical interest. Note that $\psi_1 \rightarrow \psi_2 \Rightarrow \phi_{k1} \rightarrow \phi_{k2} \Rightarrow U_1 \rightarrow U_2 \Rightarrow |U_1^* U_2| \rightarrow n$, which implies from (3-7) that $\lambda_{max}/\lambda_{min} \rightarrow \infty$.

To obtain a better understanding of the implications of (3-6) and (3-7), compare two special classes, namely:

(i) $\rho = \rho_1 = \rho_2$

Substituting in (3-6) and (3-7) yields

$$\left.\begin{aligned}
\lambda_1 &= \lambda_{n+1} = \rho(n + |U_1^* U_2|) \\
\lambda_2 &= \lambda_{n+2} = \rho(n - |U_1^* U_2|) \\
\lambda_m &= 0 \quad \text{otherwise} \quad .
\end{aligned}\right\} \qquad (3\text{-}8)$$

13

$$\frac{\lambda_{max}}{\lambda_{min}} = \frac{1 + |U_1^* U_2|/n}{1 - |U_1^* U_2|/n} \quad . \tag{3-9}$$

(ii) $\rho_1 \gg \rho_2$

Making first-order approximations in (3-6) and (3-7) it can be seen that

$$\left. \begin{array}{l} \lambda_1 = \lambda_{n+1} \simeq n\rho_1 \\[2em] \lambda_2 = \lambda_{n+2} \simeq n\rho_2 \left[1 - \frac{|U_1^* U_2|^2}{n^2} \right] \\[2em] \lambda_m = 0 \quad \text{otherwise} \quad . \end{array} \right\} \tag{3-10}$$

$$\frac{\lambda_{max}}{\lambda_{min}} = \frac{\rho_1}{\rho_2} \left[\frac{1}{1 + |U_1^* U_2|/n} \right] \cdot \left[\frac{1}{1 - |U_1^* U_2|/n} \right] \quad . \tag{3-11}$$

When $|U_1^* U_2|/n$ approaches 1 it is seen from (3-9) and (3-11) that the eigenvalue disparity (i.e., the ratio $\lambda_{max}/\lambda_{min}$) increases without bound, regardless of the disparity in jammer power levels (i.e., the ratio ρ_1/ρ_2). The eigenvalue disparity in (3-11) is approximately 0.25 ρ_1/ρ_2 times the eigenvalue disparity in (3-9). It may be observed from (3-10) that the high-power jammer determines the largest eigenvalue. This implies [according to (3-3)] that the high-power jammer is attenuated quickly. From (3-10) it is also seen that the smaller eigenvalue is determined by the low-power jammer, by the angular separation between

14

the jammers, and by the array configuration. Thus for $|U_1^* U_2|/n$
approaching 1, we see that this eigenvalue becomes quite small. This
explains why the low-power jammer was attenuated very slowly in Fig. 2-2.

When $|U_1^* U_2|/n$ approaches 0 it is seen from (3-8) that both the
eigenvalues are the same and hence the ratio $\lambda_{max}/\lambda_{min}$ approaches 1,
the same ratio in class (ii) becomes only ρ_1/ρ_2.

To summarize the above, it may be stated that the eigenvalue
disparity varies between ρ_1/ρ_2 and ∞ as the $|U_1^* U_2|/n$ varies between 0
and 1. $|U_1^* U_2|/n$ in turn depends upon the angular positions (ψ_1, ψ_2) of
the two jammers and on the number of antenna elements and their
geometrical arrangement. For a given range of values of ψ_1 and ψ_2,
the number of elements and their arrangement may be chosen such that
$|U_1^* U_2|/n$ may be kept small, which in turn will keep the eigenvalue
disparity near the jammer power disparity.

Examples of various array configurations are examined in the next
section in order to study their effect on the eigenvalue disparity.

15

IV. ESTIMATING RELATIVE CONVERGENCE RATES IN VARIOUS ARRAY CONFIGURATIONS

Several antenna array configurations were tried in order to study
the eigenvalue disparity for different numbers of elements and various
element configurations. One of these configurations has already been
shown in Fig. 3-1, where the element locations are shown together with
the phase shifters and the adaptive linear combiner. Other array con-
figurations are shown in the "a" parts of the figures in this section.
In these latter figures, only the element locations are shown explicitly;
phase shifting and adaptive linear combining are understood to follow the
pattern established in Figures 2-1 and 3-1.

Figure 4-1 and the "b" parts of the remaining figures in the section
are plots of the normalized eigenvalue disparity (NED), which is defined
as $[\lambda_{max}/\lambda_{min}]/[\rho_1/\rho_2]$ for the particular configuration under considera-
tion. In each case the angular position of jammer 1, i.e., ψ_1, is fixed
arbitrarily at 40° while that of jammer 2, i.e., ψ_2, is varied between
-180° and 180°. Normalized eigenvalue disparity is plotted as a function
of ψ_2.

Figure 4-1 is the NED plot for the linear array with two auxiliary
elements that was used in Section II to show that very slow convergence
can be experienced for closely spaced jammers with disparate power
levels. The particular case that was examined involved a 55° incidence
angle for the second jammer J_2. From Figure 4-1 it can be seen that the
NED for this incidence angle is approximately 45. This large eigenvalue
disparity shows why a very long adaptation period was required for this
particular antenna/signal configuration.

16

Figure 4-1 also indicates that similar convergence problems can be anticipated over a broad range of possible J_2 arrival angles. Particularly difficult convergence problems are indicated at J_2 arrival angles that approximate the J_1 arrival angle. This result runs contrary to intuition and experience since it would be expected that a single, slightly broadened null would form quickly and eliminate both jammers in such cases. Appendix D examines the apparent conflict between the results indicated by the NED plot and the results that have been observed in practice. It is shown that, almost paradoxically, both viewpoints have their validity and that the choice of viewpoint depends upon the specification of initial conditions and the definition of convergence.

The NED plot for the linear configuration of Fig. 4-2a is shown in Fig. 4-2b. This plot is very similar to that of Fig. 4-1, though the value of NED for each ψ_2 is smaller than the corresponding value in Fig. 4-1. At $\psi_2 = 55^o$, NED for the three auxiliary case is 17.1, which is 2.6 times smaller than the NED in the linear configuration with two auxiliaries. This indicates that the nulling process in the array with three auxiliaries will be correspondingly faster than that in the array with two auxiliaries.

A simple way to break the symmetry of the linear array is to use a triangular array such as that shown in Figure 4-3a. Comparing Figure 4-3b with Figs. 4-1 and 4-2b, it is evident that, in the region where $|\psi_1-\psi_2|$ is small, the normalized eigenvalue disparity (NED) is substantially less for the triangular configuration than the NED for the linear configurations with two or three auxiliary elements. As a specific example, at $\psi_2 = 55^o$ the NED for the triangular configuration is 12.5, while the NED for the linear configuration (Fig. 4-1) is 45.0.

17
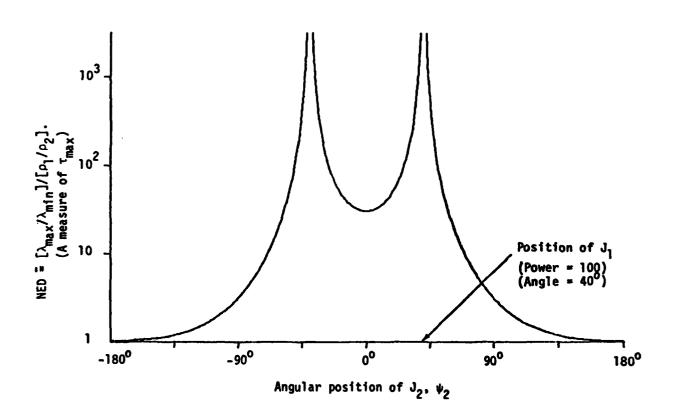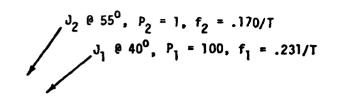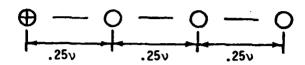
Figure 4-1. NED Plot for the Linear Array with Two Auxiliary Elements.

18

J_2 @ $55°$, $P_2 = 1$, $f_2 = .170/T$

J_1 @ $40°$, $P_1 = 100$, $f_1 = .231/T$

ν = Wavelength

$\oplus$ = Primary antenna element

O = Auxiliary antenna elem.

a)

b)

NED = $[\lambda_{max}/\lambda_{min}]/[\rho_1/\rho_2]$. (A measure of τ_{max})

10^3

10^2

10

1

$-180°$ $-90°$ $0°$ $90°$ $180°$

Angular position of J_2, ψ_2

Position of J_1
(Power = 100)
(Angle = $40°$)

.25ν .25ν .25ν
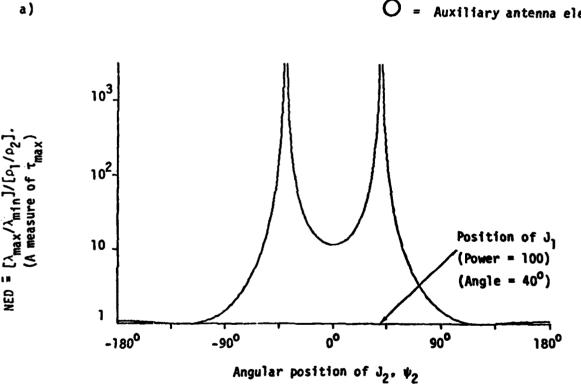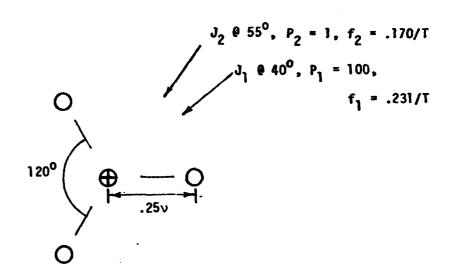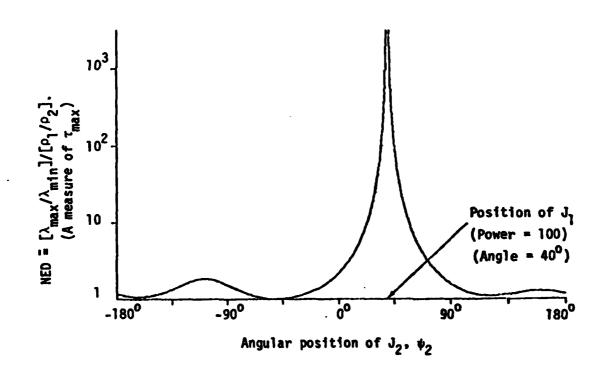
Figure 4-2.   Antenna Geometry and NED Plot for the
Linear Array with Three Auxiliary Elements.

19

J_2 @ 55°, $P_2 = 1$, $f_2 = .170/T$

J_1 @ 40°, $P_1 = 100$,

$f_1 = .231/T$

120°

.25ν

$\oplus$ = Primary antenna element

$\bigcirc$ = Auxiliary antenna element

ν = Wavelength

a)

NED $\equiv [\lambda_{max}/\lambda_{min}]/[\rho_1/\rho_2]$.
(A measure of τ_{max})

Position of J_1
(Power = 100)
(Angle = 40°)

Angular position of J_2, ψ_2

b)

Figure 4-3. Antenna Geometry and NED Plot for the Triangular Array.

20

That is, the NED in the triangular configuration is 3.6 times smaller than the NED in the linear configuration. Using the lower bound on τ_{max} [i.e., (3-5)] it is estimated that the adaptive nulling process in the triangular configuration is about 3.6 times faster than that in the linear configuration.

The hexagonal configuration of Fig. 4-4a, a natural extension of the triangular configuration just described, was also tried. In the region $-50^o \leq \psi \leq 110^o$, the NED plot shown in Fig. 4-4b appears identical to that in Fig. 4-3b. In the other regions the NED is somewhat better (i.e., smaller) than that in Fig. 4-3b. Thus the hexagonal configuration may be expected to exhibit convergence beha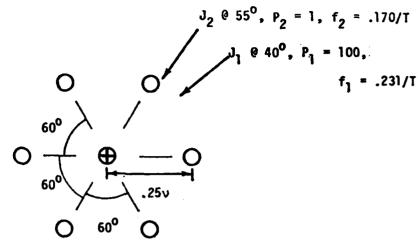vior much like the triangular. At $\psi_2 = 55^o$ the NED is the same as in the triangular case and hence the convergence rate in both cases is expected to be the same.

Next consider the configuration shown in the Fig. 4-5a, which consists of two concentric triangles. The inner triangle is the same as that of Fig. 4-3a. The outer triangle has its vertices at a radius of 7.75 wavelengths (which is 30 times the radius of the inner one). The resulting NED plot is shown in Fig. 4-5b. Except for a very small region around 40° (the position of Jammer 1) the value of NED rarely exceeds 10. For the example of $\psi_2 = 55^o$, the value of NED is 1.13. This values is approximately 11 times smaller than the corresponding NED for the single small triangle case (Fig. 4-3b). This indicates a correspondingly faster convergence rate in the two triangle case.
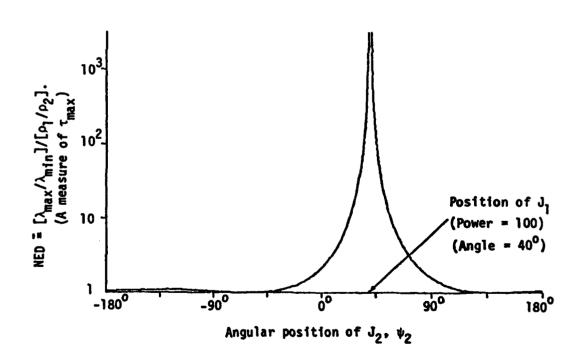
Comparing the two-triangle case (Fig. 4-5b) with the two-auxiliary-element linear configuration (Fig. 4-1) the NED in the two-triangle case is 40 times smaller than the corresponding NED in the linear case. Thus it appears that the nulling process in the two triangle case will be 40 times faster than that in the linear case.

21

J_2 @ 55°, P_2 = 1, f_2 = .170/T

J_1 @ 40°, P_1 = 100,

f_1 = .231/T

60°

60°

60°

.25ν

ν = Wavelength

⊕ = Primary antenna element

O = Auxiliary antenna elem.

a)

NED = $[\lambda_{max}/\lambda_{min}]/[\rho_1/\rho_2]$.
(A measure of τ_{max})

Position of J_1
(Power = 100)
(Angle = 40°)

Angular position of J_2, ψ_2
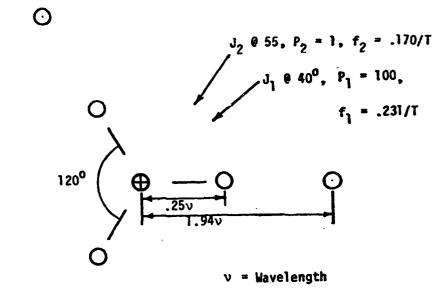
b)

Figure 4-4.   Antenna Geometry and NED Plot
for the Hexagonal Array.

22

J_2 @ 55, $P_2 = 1$, $f_2 = .170/T$

J_1 @ 40°, $P_1 = 100$,

$f_1 = .231/T$

120°

.25ν

1.94ν

ν = Wavelength

⊕ = Primary antenna element

○ = Auxiliary antenna element

a)

$NED = [\lambda_{max}/\lambda_{min}][\rho_1/\rho_2]$.
(A measure of τ_{max})

10^3

10^2

10

1

Position of J_1
(Power = 100)
(Angle = 40°)

-180°   -90°   0°   90°   180°

Angular position of J_2, ψ_2

b)

Figure 4-5. Antenna Geometry and NED Plot for the Array
Configured as two Equilateral Triangles.

23

The reasoning which led to the selection of the two-triangle case for study was as follows: It may be seen that elements spaced at a long distance from the primary element experience a large time difference in the signal. Hence *intuitively a large separation between elements (a large aperature) may tend to magnify the apparent angular separation between closely spaced jammers. This magnification tends to reduce the disparity between eigenvalues of the adaptive null steerer.*

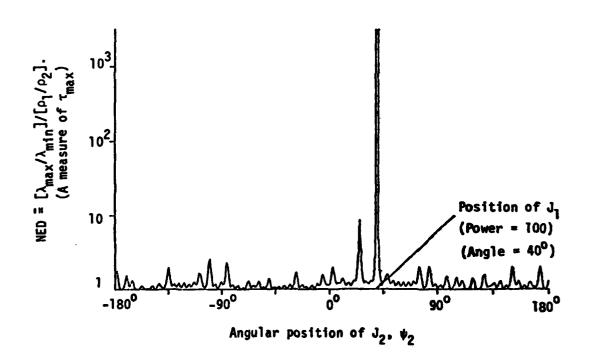As a final case for examining relative convergence rates, the three-triangle configuration of Fig. 4-6a was considered. This is an extension of the two-triangle case; the inner and outer triangles of elements remain unchanged. Figure 4-6b is the NED plot for this configuration. The NED values in this case fall generally below the NED values for the two-triangle configuration, and the strong spike at about 25° has been suppressed. The improvement is, however, relatively small at most angles. In particular, the NED value at $\psi_2 = 55^{\circ}$ is 1.09, an insignificant improvement over the value of 1.13 that was obtained with the two-triangle arrangement. It appears that convergence for the three-triangle case will be about 41 times faster than the convergence performance exhibited by the linear array with two auxiliaries.

The eigenvalue disparities have been discussed for various array configurations based upon arrangements of elements in simple linear and triangular patterns. The eigenvalue disparity is related to the time constant τ_{max} of the slowest mode when adapting with the value of μ giving the highest convergence rate, in accord with equation (3-5). The results obtained from the simulations given in the following section confirm that the eigenvalue disparity can provide useful information about convergence rate.

24

a)

J_2 @ 55°, $P_2 = 1$, $f_2 = .170/T$

J_1 @ 40°, $P_1 = 100$,

$f_1 = .231/T$

120°

.25ν

1.94ν

7.75ν

ν = Wavelength

$\bigoplus$ = Primary antenna element

$\bigcirc$ = Auxiliary antenna element

Position of J_1
(Power = 100)
(Angle = 40°)

$NED = [\lambda_{max}/\lambda_{min}]/[\rho_1/\rho_2]$.
(A measure of τ_{max})

Angular position of J_2, ψ_2

b)
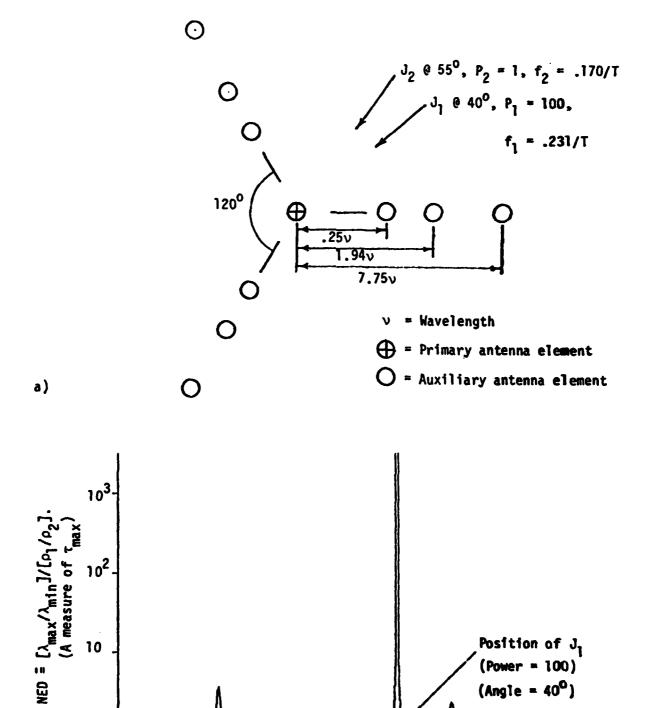
Figure 4-6. Antenna Geometry and NED Plot for the Array
Configured as Three Equilateral Triangles.

25

V. SIMULATION RESULTS

The principal thrust of this section will be the discussion of
convergence rate and a comparison of simulation results with the
estimates from the foregoing section. The beam patterns at convergence
will also be documented in this section for each antenna configuration.
Discussion of the beam patterns will, however, be deferred until
Section VII where the discussion can include material related to the
optimal beam pattern as well as the simulation results.

Simulations for the cases discussed in Section IV were conducted
in a manner similar to that described in Section II for the linear array
with two auxiliary elements. The same simulation program was applied
to all the arrays, and the number of adapts required to reduce output
power below 1×10^{-6} was determined for each array configuration.
Additionally, the beam pattern at convergence was plotted for each case.

Much of the data concerning convergence rate characteristics for
the different array configurations is summarized in Table 1. The
columns at the left side of the table describe the array configurations
and give cross references to the figures that illustrate each geometry.
The center section of the table brings forward the pertinent information
from the normalized eigenvalue disparity (NED) curves of Section IV for
the particular case of interest, i.e., for jammer azimuths of 40° and
55°. Additionally, this section shows the relative convergence rates
with the baseline configuration taken as the linear array with two
auxiliary elements. The right side of the table gives a summary of the
simulation data. The adaptation constant is shown for each case
together with the observed number of adaptations for convergence and

26

Table I

CONVERGENCE RATE CHARACTERISTICS OF VARIOUS ARRAY CONFIGURATIONS

Array Configuration			Estimated Convergence Rates Based on τ_{max}		Simulation Data and Results		
Figure No.	Geometry of Auxiliary Elements	No. of Auxiliary Elements	NED $\equiv$ $[\lambda_{max}/\lambda_{min}]/[\rho_1/\rho_2]$ at $\psi_1=40^o$, $\psi_2=55^o$	Relative Converg. Rates[†]	μ Used	No. of Adapts for Converg.	Relative Converg. Rates[‡]
Fig. 2-1	Line	2	44.97	1.0	1×10^{-3}	141,000	1.0
Fig. 4-2	Line	3	17.11	2.6	0.67×10^{-3}	50,000	2.8
Fig. 4-3	Triangle	3	12.50	3.6	0.67×10^{-3}	26,100	5.4
Fig. 4-4	Hexagon	6	12.50	3.6	0.33×10^{-3}	25,890	5.4
Fig. 4-5	Two concentric triangles	6	1.13	39.8	0.33×10^{-3}	4,130	34.1
Fig. 4-6	Three concentric triangles	9	1.09	41.3	0.22×10^{-3}	4,030	35.0

[†] Estimated relative convergence rate $\overset{\Delta}{=}$ $\dfrac{\text{NED for linear array with 2 auxiliary elements}}{\text{NED for the configuration under consideration}}$

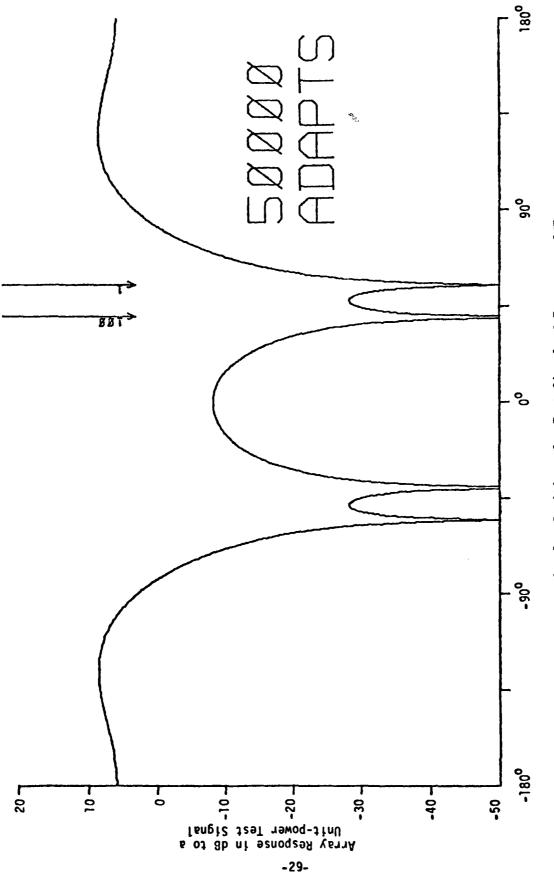[‡] Observed relative convergence rate $\overset{\Delta}{=}$ $\dfrac{\text{No. of adapts for linear array with 2 aux. elem.}}{\text{No. of adapts for the config. under consideration}}$

an observed relative convergence rate. Once again, the relative convergence rate is based upon the convergence rate of the linear array with two auxiliary elements.

Appropriate selection of the adaptation constant μ was an important consideration in conducting the simulation experiments. The major concern was to assure that convergence times could be meaningfully compared for the various array configurations; this was accomplished by setting the adaptation constant experimentally for the linear array with two auxiliary elements, and then adjusting the adaptation constant for other cases so that the product of μ and the array input power remained a constant. The value of $\mu = 1 \times 10^{-3}$ was selected for the linear array with two auxiliary elements by conducting a few experimental runs. A smaller value of μ resulted in a slower convergence rate than that shown earlier in Figure 2-2, with no improvement in the pattern. A larger value of μ resulted in poor beam patterns due to increased mis-adjustment in the weight vector [see Widrow 8]. For other array configurations listed in the table, μ was set inversely proportional to the number of auxiliary elements in each case. If μ were set smaller than shown in the table, the adaptive nulling process would be slower than that obtained with the given μ, without any improvement in the beam pattern. If μ were set larger, the beam pattern would deteriorate in comparison with that obtained with the given μ.

From Table 1 it is seen that the linear configuration with three auxiliaries converged 2.8 times faster than the case in Fig. 2-1. This is slightly faster than that estimated on the basis of eigenvalue disparity. The converged beam pattern (Fig. 5-1) is similar to that in Fig. 2-2d. The pattern shows similar notches in the jammer positions, and it is slightly better in other regions.

28

50000
ADAPTS

Angular Position of a Test Signal of Frequency .2/T

Array Response in dB to a Unit-power Test Signal

Figure 5-1. Converged Beam Pattern for the Linear Array with Three Auxiliary Elements (Figure 4-2a).

For the triangular array configuration, the observed convergence rate is 5.4 times faster than that for the linear configuration of Fig. 2-1. It may be noted that the observed convergence rate is substantially faster than that estimated in Section IV by comparison of the eigenvalue disparity. The converged beam pattern is shown in Fig. 5-2.

The results of simulation of the hexagonal configuration are essentially the same as those for the triangular. The convergence rate is the same as for the triangular case. The beam pattern (Fig. 5-3) is strikingly similar to that shown in Fig. 5-2.

The observed convergence rate in the two-concentric-triangle configuration is about 34 times faster than that in the case in Fig. 2-1. This rate is slightly lower than estimated on the basis of eigenvalue disparity. The converged beam pattern is shown in Fig. 5-4.

The final configuration that was examined was the three-concentric-triangle case. The estimates of convergence rate indicated that performance would be only slightly better than that given by the two-concentric-triangle case. In the simulation a minor improvement of 100 adaptations was obtained over the number of adaptations needed in the two-concentric-triangle case. The beam pattern for the configuration of three concentric triangles is shown in Fig. 5-5.

Figure 5-2. Converged Beam Pattern for the Array with Auxiliary Elements Configured as an Equilateral Triangle (Figure 4-3a).

31

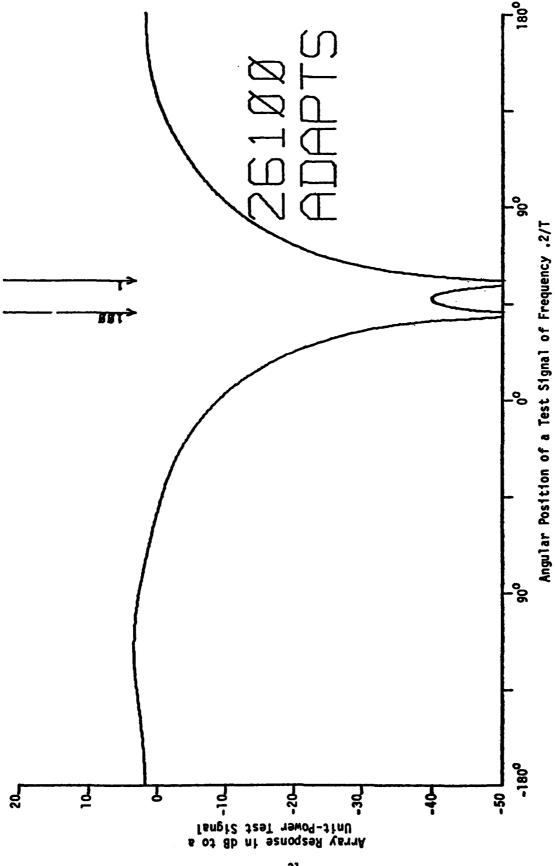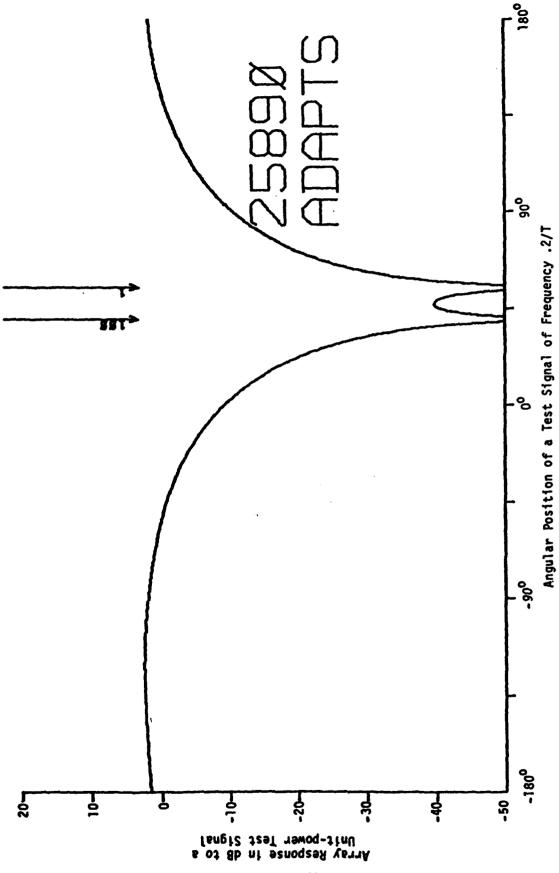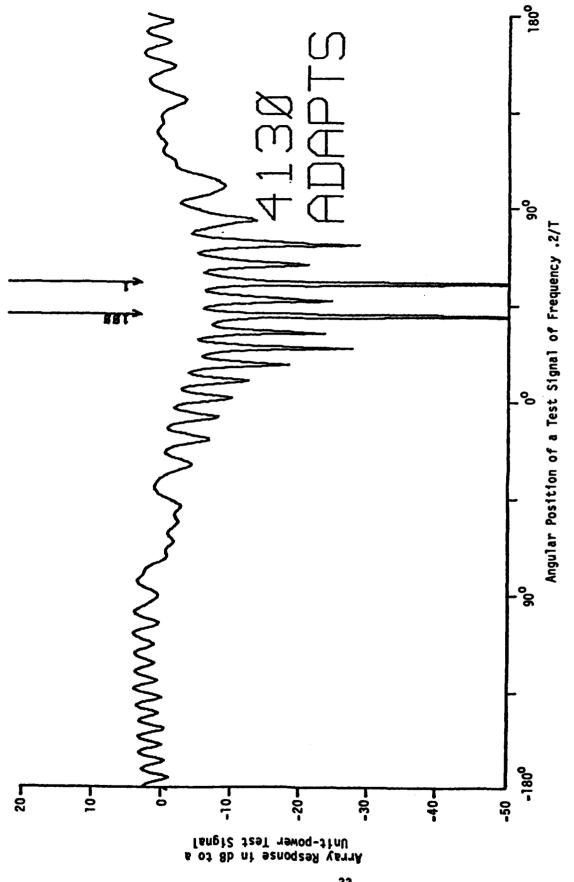Figure 5-3. Converged Beam Pattern for the Hexagonal Array (Figure 4-4a).

Figure 5-4. Converged Beam Pattern for the Array with Auxiliary Elements Configured as Two Concentric Triangles (Figure 4-5a).
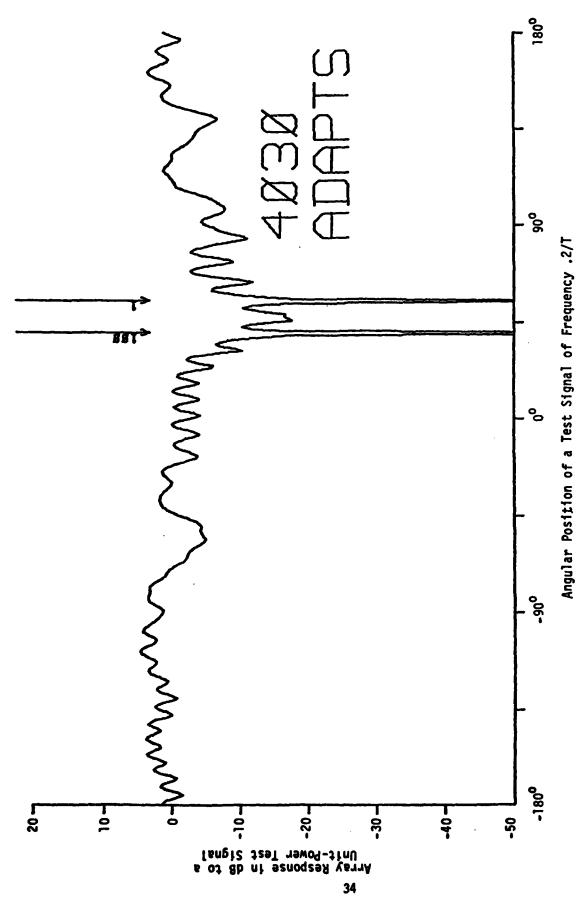
Figure 5-5. Converged Beam Pattern for the Array with Auxiliary Elements configured as Three Concentric Triangles (Figure 4-6a).

34

VI. DERIVATION OF OPTIMAL BEAM PATTERN

A closed form solution for the beam pattern of the adaptive antenna array of Fig. 3-1 will now be found.

Let W be the weight vector defined as

$$W = [w_1 \ w_2 \ w_3 \ \dotsc \ w_{2n}]^T \qquad (6\text{-}1)$$

where w_i and w_{i+n} (i=1...n) represent the in-phase and quadrature phase weights at element i. Let X be the vector of received signals at each element. Then

$$X = [x_1 \ x_2 \ \dotsc \ x_n \ \dotsc \ x_{2n}]^T \qquad (6\text{-}2)$$

where the x_i and $x_{(i+n)}$ (i=1...n) represent the in-phase and quadrature phase components of the signal at element i. Also let x_0 be the signal with power ρ at the primary element.

The output of the antenna array is given as

$$y = x_0 - W^T \cdot X \qquad . \qquad (6\text{-}3)$$

Consequently, the output power becomes

$$E[y^2] = \rho - 2W^T E[x_0 X] + W^T E[X \cdot X^T] \ W \qquad . \qquad (6\text{-}4)$$

Define

$$P = E[x_0 \cdot X]$$

and

$$R = E[X \cdot X^T] \qquad .$$

35

Derivation of the sensitivity pattern for the array depicted in Figure 3-1 is achieved as follows. Assume a sinusoidal plane wave of power ρ and angle ψ incident on the array. Then it can be shown that

$$E[x_j \cdot x_k] = \cos(\phi_j - \phi_k) \qquad (6\text{-}6)$$

where

$$\phi_k = \begin{cases} 0 & k = 0 \\ 2\pi \cdot \ell_k \cos(\alpha_k - \psi) & \ell \leq k < n \\ 2\pi \cdot \ell_{k-n} \sin(\alpha_{k-n} - \psi) & n + 1 \leq k \leq 2n \end{cases} \qquad (6\text{-}7)$$

Therefore

$$P(\psi) = \begin{bmatrix} p_1(\psi) \\ p_2(\psi) \\ \vdots \\ p_{2n}(\psi) \end{bmatrix} = E \begin{bmatrix} x_0 x_1 \\ x_0 x_2 \\ \vdots \\ x_0 x_{2n} \end{bmatrix} \qquad (6\text{-}8)$$

and

$$R(\psi) = E[x_i x_j] = E \begin{bmatrix} x_1 x_1 & x_1 x_2 & \cdots & x_1 x_{2n} \\ \vdots & & & \\ \vdots & & & \\ x_{2n} x_1 & \cdots & & x_{2n} x_{2n} \end{bmatrix} \qquad (6\text{-}9)$$

Hence, given the geometry of the array and the arrival angle of the test signal, P and R can easily be calculated.

In Appendix B it is shown that

$$W_{opt} = \left[\sum_{k=1}^{r} \frac{Q_k Q_k^T}{\lambda_k + \sigma_N^2} \right] \cdot P_{jammer} \qquad (6\text{-}10)$$

where Q_k is the kth eigenvector and λ_k is the kth eigenvalue of R_{jammer}, as defined in Appendix C. Recall, also, that σ_N^2 is the power of the isotropic white noise incident upon every element. The vector P_{jammer}, is similar in structure to the P defined in Eq. (6-8). Specifically, it is determined by M independent jammers, in the following manner.

$$P_{jammer} = \sum_{i=1}^{M} P(\psi_i) \qquad (6\text{-}11)$$

where ψ_i is the arrival angle of jammer i. $P(\psi_i)$ is defined by Eqs. (6-5,6-6,6-7). Substituting (6-10) into (6-3) yields

$$E[y^2] = \rho - P_{jammer}^T \left[\sum_{k=1}^{r} \frac{Q_k Q_k^T}{\lambda_k + \sigma_N^2} \right] \cdot P_{jammer} \qquad (6\text{-}12)$$

$$+ P_{jammer} \left[\sum_{k=1}^{r} \frac{Q_k \cdot Q_k^T}{\lambda_k + \sigma_N^2} \right] \cdot R \cdot \left[\sum_{k=1}^{r} \frac{Q_k \cdot Q_k^T}{\lambda_k + \sigma_N^2} \right] \cdot P_{jammer} \cdot$$

Once the eigenvectors and eigenvalues are established, Eq. (6-12) specifies the optimal beam pattern. Note that the above analysis is true for M jammers. Appendix A derives eigenvectors and eigenvalues for the two jammer case.

37

VII. BEAM PATTERN CHARACTERISTICS

To compare the converged beam patterns of different antenna configurations, a desired beam pattern must be established. For this study, the desired beam pattern is unity gain in all directions except where a jammer is incident on the array, where the gain should approach zero.

In section VI, a closed form expression for the converged beam pattern was derived. That expression was used to develop a program for directly generating the converged pattern for a particular array. The simulation results of Fig. 2-2d, took 141,000 adapts to converge. This represents a substantial amount of computer time. The closed form solution was used to generate the pattern of Fig. 7-1a, verifying the simulation results. Much less computer time was required to generate this pattern than to generate the simulation results. The program using the closed-form expression allowed quick comparison of converged beam patterns for different array configurations.

Converged beam patterns for two basic antenna geometries, linear and triangular, will be discussed. The linear array consists of omni-directional antenna elements placed on a line. As mentioned previously, a linear array results in undesired symmetric nulls. By adding additional equally spaced elements, extra degrees of freedom are introduced into the system. As can be seen in Figures 7-1a, b, c the additional array elements cause the nulls to become sharper, and introduce increasing ripple into the beam pattern. The gain in the region between the two jammers comes closer to unity as the number of elements is increased.

a) Linear array of three elements separated by .25ν

b) Linear array of six elements separated by .25ν

c) Linear array of nine elements separated by .25ν
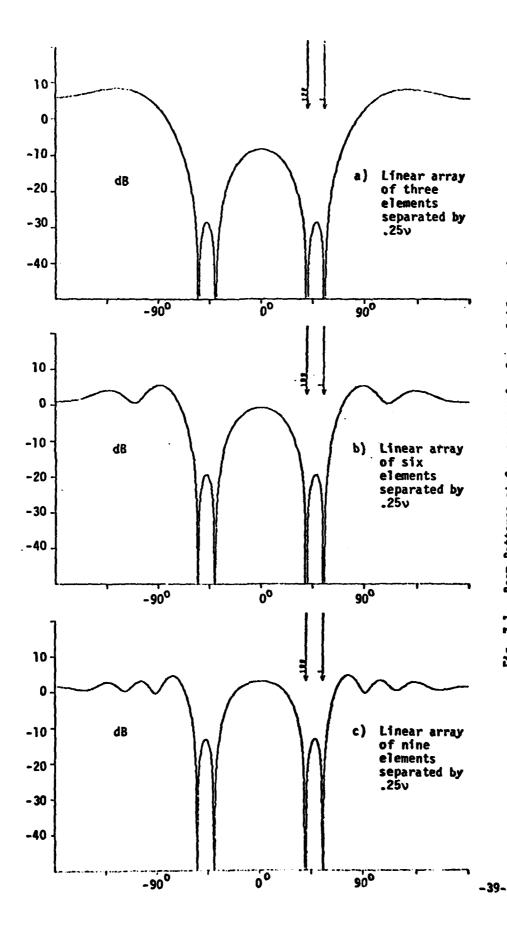
Fig. 7-1. Beam Patterns at Convergence for Several Linear Arrays.

-39-

The triangular arrays consist of antenna elements positioned as shown in Figures 4-3a (3 elements), 4-9a (6 elements), and 4-6a (9 elements). Each of the latter two figures builds upon its predecessor by adding three additional elements. Note in Figures 7-2a, b, c that the undesirable symmetric nulls are no longer present. As with the linear arrays, as the number of elements is increased, the nulls sharpen, and ripple is introduced.

Generally, increasing the number of auxiliary antenna elements sharpens the nulls, in addition to increasing the convergence rate. A triangular array eliminates the unwanted symmetric nulls.
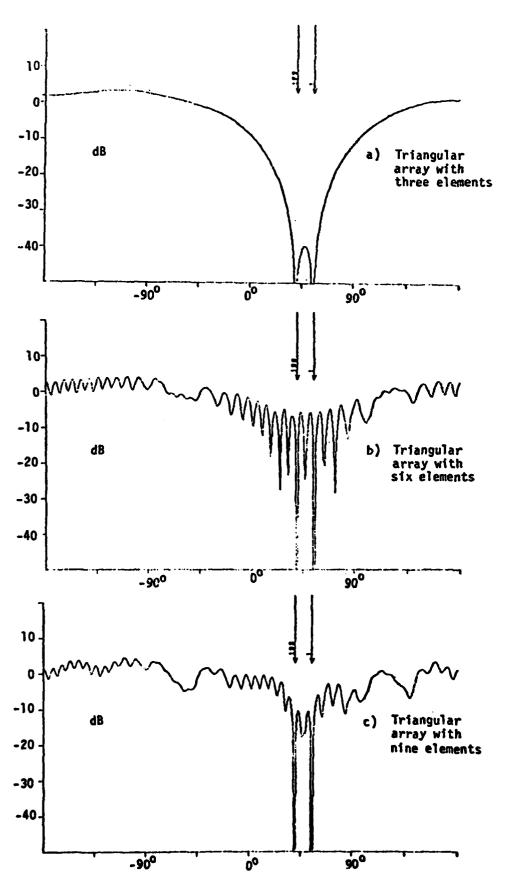
Figure 7-2. Beam Patterns at Convergence for Several Triangular Arrays.

a) Triangular array with three elements

b) Triangular array with six elements

c) Triangular array with nine elements

VIII. CONCLUSIONS AND DIRECTIONS FOR FURTHER STUDY

It has been demonstrated that the addition of a few surplus auxiliary elements can effect a substantial improvement in the convergence rate of an adaptive antenna array subjected to two closely spaced jammers of disparate power level. A theoretical analysis showed that the normalized eigenvalue disparity provided a good measure of adaptation rate for any given configuration. Computer simulations confirmed the validity of the analysis and furnished specific illustrations of array geometries with convergence rates far better than that exhibited by a minimal linear array. Additional work is needed to provide more specific design guidance for arrays with good convergence properties. It would be useful to examine the question of optimal convergence rate for the two-jammer case, given some set of constraints on array dimensions and element count.

Considerable progress has been made in developing a technique for studying the impact of antenna geometry on the converged beam pattern in the two-jammer case. The closed-form expression for computation of the beam pattern provided an efficient way to determine the pattern for any element geometry that might be under consideration. Further work is needed, however, to provide better insight into the synthesis of arrays with good beam-pattern properties.

The concepts and results of this paper could also be extended to the 3-dimensional case, where jammers and array elements are no longer coplanar. This will require techniques for representing the 3-dimensional beam pattern in 2 dimensions. Consideration of the 3-dimensional extensions has begun.

Extension of these results to arrays containing many more than three or four elements will be undertaken. New approximation methods will be required to keep the algebraic expressions tractable and insightful.

IX. REFERENCES

1. B. Widrow, P. E. Mantey, L. J. Griffiths and B. B. Goode, "Adaptive Antenna Systems," Proc. IEEE, vol. 55, pp. 2143-2159, Dec. 1967.

2. C. L. Zahm, "Application of Adaptive Arrays to Suppress Strong Jammers in the Presence of Weak Signals," IEEE Trans. on Aerospace and Electronic Systems, vol. AES-9, pp. 260-271, March 1973.

3. L. J. Griffiths, "A Simple Adaptive Algorithm for Real-time Processing in Antenna Arrays," Proc. IEEE, vol. 57, pp. 1696-1704, Oct. 1969.

4. O. L. Frost, "An Algorithm for Linearly Constrained Adaptive Array Processing," Proc. IEEE, Vol. 60, pp. 926-935, Aug. 1972.

5. W. D. White, "Cascade Preprocessors for Adaptive Antennas," IEEE Trans. Antenna and Propagation, vol. AP-24, pp. 670-684, Sept. 1976.

6. I. S. Reed, J. D. Mallet and L. E. Brennan, "Rapid Convergence Rate in Adaptive Arrays," IEEE Trans. Aerospace and Electronic Systems, vol. AES-10, pp. 853-863, Nov. 1974.

7. B. Widrow, J. M. McCool, M. G. Larimore and R. Johnson, Jr., "Stationary and Nonstationary Learning Characteristics of the LMS Adaptive Filter," Proc. IEEE, vol. 64, pp. 1151-1162, Aug. 1976.

8. B. Widrow and J. McCool, "A Comparison of Adaptive Algorithms Based on the Methods of Steepest Descent and Random Search," IEEE Trans. Antennas and Propagation, Vol. AP-24, No. 5, Sept. 1976.

APPENDIX A

The purpose of this Appendix is to obtain explicit expressions for the eigenvalues and eigenvectors of the adaptive antenna array of Fig. 3.

Let the two jammers arriving at ψ_1 and ψ_2 be sinusoids. Let the weights attached directly to the antenna elements be labeled 1 through n, and those attached after the -90° phase shift be correspondingly labeled $n + 1$ through $2n$. See Fig. 3.

The signal at the input to k^{th} weight is given by

$$
\begin{aligned}
x_k = \ & 2\rho_1 \cos(\omega_1 t + \theta_1 - \phi_{k1}) \\[1ex]
& + \ 2\rho_2 \cos(\omega_2 t + \theta_2 - \phi_{k2})
\end{aligned}
$$

where, for $i = 1, 2$ we have

$\rho_i \triangleq$ Jammer power i at each ant. ele.

$\omega_i \triangleq$ Radian frequency of jammer 1.

$\theta_i \triangleq$ Uniformly distributed $[0,2\pi]$ random phase of the jammer i at the primary element. (θ_1 is statistically independent of θ_2.)

$$
\phi_{ki} = \begin{cases} 2\pi\ell_k \cos(\psi_i - \alpha_k) & \text{for } k = 1, \ldots n \\[2ex] 2\pi\ell_{k-n} \cos(\psi_i - \alpha_{k-n}) - \dfrac{\pi}{2} \\[2ex] \text{for } k = n+1, \ldots, 2n \quad . \end{cases}
$$

(A1)

It can be seen that

$$E(x_j x_k) = \rho_1 \cos(\phi_{j1} - \phi_{k1}) + \rho_2 \cos(\phi_{j2} - \phi_{k2})$$

$$\text{for } j, k = 1, \ldots, 2n \qquad \text{(A2)}$$

The correlation matrix R is defined by

$$R \triangleq [E(x_j x_k)] \qquad . \qquad \text{(A3)}$$

Substituting from (A1) and (A2):

$$R = \begin{bmatrix} C_1 + C_2 & +(D_1 + D_2) \\ -(D_1 + D_2) & C_1 + C_2 \end{bmatrix} \qquad \text{(A4)}$$

where C_1, C_2, D_1 and D_2 are nxn matrices given by

$$[C_i]_{jk} = \rho_i \cos(\phi_{ji} - \phi_{ki})$$

$$[D_i]_{jk} = \rho_i \sin(\phi_{ji} - \phi_{ki})$$

$$i = 1, 2$$

$$j, k = 1, \ldots, n \qquad .$$

Using the theorem derived in Appendix C, the eigenvalues of R are related to the eigenvalues of a complex matrix B given by

$$B \triangleq C_1 + C_2 + i[-(D_1 + D_2)] \qquad \text{(A5)}$$

in the following manner: n eigenvalues (say $\lambda_1, \lambda_2, \ldots, \lambda_n$) of R are the same as those of B. The remaining n eigenvalues are related as follows:

46

$$\lambda_k = \lambda_{k-n} \quad \text{for} \quad k = n+1, \ldots, 2n \quad . \tag{A6}$$

Writing B in terms of vector outer products of complex exponential vectors:

$$B = \rho_1 U_1 U_1^* + \rho_2 U_2 U_2^* \tag{A7}$$

where

$$U_j = \left[e^{-i\phi_{1j}}, e^{-i\phi_{2j}}, \ldots, e^{-i\phi_{nj}} \right]^T \quad j = 1, 2 \quad . \tag{A8}$$

It can be seen that the rows of the Hermetian matrix $U_j U_j^*$ are linearly dependent. Thus $U_j U_j^*$ is of rank 1, with one real eigenvalue, and all other eigenvalues are zero. Since the columns of $U_j U_j^*$ are also all linearly dependent on U_j, U_j spans the eigenspace corresponding to the one nonzero eigenvalue of $U_j U_j^*$.

Since B is a linear combination of $U_1 U_1^*$ and $U_2 U_2^*$, B will be of rank ≤ 2 for $n \geq 2$ with at most two positive eigenvalues. The eigenvectors of B will be in the space spanned by U_1 and U_2. Thus an eigenvector is given by

$$\Gamma = \gamma_1 U_1 + \gamma_2 U_2 \tag{A9}$$

where γ_1 and γ_2 are complex scalars to be determined from the following derivation.

Combining (A7) and (A9),

$$B\Gamma = \gamma_1 U_1 \left[\rho_1 \left(n + \frac{\gamma_2}{\gamma_1} U_1^* U_2 \right) \right] + \gamma_2 U_2 \left[\rho_2 \left(n + \frac{\gamma_1}{\gamma_2} U_2^* U_1 \right) \right] \quad . \tag{A10}$$

47

Since $B\Gamma = \lambda\Gamma$, for Γ to be an eigenvector

$$\lambda = \rho_1 n + \frac{\gamma_2}{\gamma_1} U_1^* U_2 = \rho_2 n + \frac{\gamma_1}{\gamma_2} U_2^* U_1 \quad . \tag{A11}$$

Solving (A11), a quadratic in $\frac{\gamma_2}{\gamma_1}$;

$$\frac{\gamma_2}{\gamma_1} = \frac{\frac{n}{2}(\rho_1+\rho_2) + \left[\frac{n^2}{4}(\rho_2-\rho_1)^2 + \rho_2\rho_1 |U_1^* U_2|^2\right]^{\frac{1}{2}}}{\rho_1 U_1^* U_2} \quad . \tag{A12}$$

Substituting (A12) in (A11) and using (A6),

$$
\left.
\begin{aligned}
\lambda_1 &= \frac{n}{2}(\rho_1+\rho_2) + \left[\frac{n^2}{4}(\rho_1-\rho_2)^2 + \rho_1\rho_2 |U_1^* U_2|^2\right]^{\frac{1}{2}} \\[2mm]
\lambda_2 &= \frac{n}{2}(\rho_1+\rho_2) - \left[\frac{n^2}{4}(\rho_1-\rho_2)^2 + \rho_1\rho_2 |U_1^* U_2|^2\right]^{\frac{1}{2}} \\[2mm]
\lambda_{n+1} &= \lambda_1; \; \lambda_{n+2} = \lambda_2 \\[2mm]
\lambda_m &= 0 \text{ for } m \notin \{1, 2, n+1, n+2\} \quad .
\end{aligned}
\right\} \tag{A13}
$$

Thus (A13) yields the eigenvalues for the configuration of Fig. 3.

By the theorem of Appendix C, the eigenvectors of R can be expressed in terms of the eigenvectors of B, which will now be found.

Rearranging (A9):

$$\Gamma = \gamma_1\left(U_1 + \frac{\gamma_2}{\gamma_1} U_2\right)$$

From (A12);

let

$$b_1 \triangleq \frac{n}{2}(\rho_2 - \rho_1) + \left[\frac{n^2}{4}(\rho_2 - \rho_1)^2 + \rho_1 \rho_2 |U_1^* U_2|^2\right]^{\frac{1}{2}}$$

corresponding to λ_1 (A14)

and

$$b_2 \triangleq \frac{n}{2}(\rho_2 - \rho_1) - \left[\frac{n^2}{4}(\rho_2 - \rho_1)^2 + \rho_1 \rho_2 |U_1^* U_2|^2\right]^{\frac{1}{2}}$$

corresponding to λ_2 .   (A15)

Then

$$\left.\frac{\gamma_2}{\gamma_1}\right| = \frac{b_1}{\rho_1 U_1^* U_2}$$
for λ_1

and

$$\left.\frac{\gamma_2}{\gamma_1}\right| = \frac{b_2}{\rho_1 U_1^* U_2} \qquad .$$
for λ_2

Thus the two eigenvectors are

$$y_1 = \lambda_1 \left(U_1 + \frac{b_1}{\rho_1 U_1^* U_2} U_2\right)$$

$$y_2 = \lambda_1 \left(U_1 + \frac{b_2}{\rho_1 U_1^* U_2} U_2\right) \quad .$$

Since the eigenvector can be linearly scaled, multiply both sides by $\dfrac{\rho_1 U_1^* U_2}{\gamma_1}$, yielding the eigenvectors of the B matrix of (A5) as

$$\Gamma_1 = (\rho_1 U_1^* U_2)\, U_1 + b_1 U_2 \qquad\qquad \text{(A16)}$$

$$\Gamma_2 = (\rho_1 U_1^* U_2)\, U_1 + b_2 U_2 \qquad . \qquad \text{(A17)}$$

Applying the theorem of Appendix C, we can find the unnormalized eigenvectors of the R matrix as:

$$Q_1 = \begin{bmatrix} \text{Re}(\Gamma_1) \\ \hline \text{Im}(\Gamma_2) \end{bmatrix}; \quad Q_{n+1} = \begin{bmatrix} -\text{Im}(\Gamma_1) \\ \hline \text{Re}(\Gamma_1) \end{bmatrix}$$

corresponding to λ_1 and λ_{n+1}

$$Q_2 = \begin{bmatrix} \text{Re}(\Gamma_2) \\ \text{Im}(\Gamma_2) \end{bmatrix}; \quad Q_{n+2} = \begin{bmatrix} -\text{Im}(\Gamma_2) \\ -\text{Re}(\Gamma_2) \end{bmatrix}$$

corresponding to λ_2 and λ_{n+2}

$$\text{(A18)}$$

(A18) expresses the eigenvectors for the configuration of Fig. 3-1.

APPENDIX B

The purpose of this appendix is to derive the optimal weight vector, W_{opt}, which minimizes the output power of the antenna array given in Fig. 1.

The output power of this array (Eq. 3-3 of the main text) is:

$$\xi = E[y^2] = \rho - 2W^t P + W^t R W \quad . \quad\quad (B1)$$

Since $\xi \geq 0$, R must be positive definite or positive semidefinite. Consequently ξ is minimized by finding the weight vector which satisfies

$$\frac{\partial \xi}{\partial w} = 0 \quad . \quad\quad (B2)$$

Differentiating Eq. B1 with respect to W gives

$$\frac{\partial \xi}{\partial w} = -2P + 2RW \quad . \quad\quad (B3)$$

Therefore,

$$W_{opt} = R^{-1} P \quad . \quad\quad (B4)$$

Addition of isotropic white noise of power σ_n^2 to the system results in

$$W_{opt} = [R + \sigma_N^2 I]^{-1} P \quad . \quad\quad (B5)$$

Since R is positive semidefinite, it can be diagonalized using an orthonormal set of eigenvectors. Let the first r eigenvalues be

non-zero, and denote the corresponding r unit eigenvectors by $Q_1, Q_2, \ldots, Q_r$. Choose the remaining n-r eigenvectors such that they are orthonormal, and span the null space of R.

The matrix which diagonalizes R is

$$Q = [Q_1\ Q_2\ \cdots\ Q_r\ \cdots\ Q_n] \quad . \tag{B6}$$

Note that

$$Q^t Q = QQ^t = I \tag{B7}$$

and define

$$W' = Q^t W \quad ; \quad W = QW' \tag{B8}$$

$$X' = Q^t X \quad ; \quad X = QX' \quad . \tag{B9}$$

Let n_i denote the white noise component of the signal on element i. Now,

$$P = E[(x_0 + n_0)(X + \begin{bmatrix} n_1 \\ \vdots \\ n_n \end{bmatrix})]$$

$$= E[x_0 X]$$

$$= E[x_0 QX']$$

$$= QE[x_0 X'] \tag{B10}$$

and define

$$P' = E[x_0 X'] \tag{B11}$$

therefore,

$$P' = Q^t P \quad ; \quad P = QP' \quad . \tag{B12}$$

52

Next, define

$$\Lambda = \text{diag}[\lambda_1, \lambda_2, \ldots, \lambda_r, 0, \ldots, 0]$$

$$= Q^t R_{xx} Q$$

$$= Q^t E[XX^t] Q$$

$$= E[Q^t X (Q^t X)^t]$$

$$= E[X'(X')^t] \tag{B13}$$

$$\lambda_i = E[(x_i')^2] \quad . \tag{B14}$$

For $r < i \leq n$, we have

$$\lambda_i = 0 \Rightarrow E(x_i')^2] = 0 \tag{B15}$$

$$x_i' = 0 \quad \text{for} \quad r < i \leq n \quad . \tag{B16}$$

Hence, the ith component of P' is given by

$$P_i' = E[x_0 x_i']$$

$$= E[x_0\ 0] \quad \text{for} \quad r + 1 \leq i \leq n \tag{B17}$$

$$\Rightarrow P_i' = 0 \quad \text{for} \quad r + 1 \leq i \leq n \quad . \tag{B18}$$

Combining Eqs. (B5,B7,B8) gives,

$$W' = Q^t W$$

$$= Q^t [R_{xx} + \sigma_N^2 I]^{-1} QQ^t P$$

$$= [\Lambda + \sigma_N^2 I]^{-1} P' \quad . \tag{B19}$$

From Eq.(B18), $P_i' = 0$ for $r + 1 \leq i \leq n$, so

$$W = \begin{bmatrix} P_1'/(\lambda_1 + \sigma_N^2) \\ P_2'/(\lambda_2 + \sigma_N^2) \\ \vdots \\ P_r'/(\lambda_r + \sigma_N^2) \\ 0 \\ \vdots \end{bmatrix} \quad . \qquad (B20)$$

If follows from Eq. (B12) that

$$P_k' = Q_k^t P \qquad (B21)$$

and so

$$w_k' = \begin{cases} Q_k^t P/(\lambda_k + \sigma_N^2) & 1 \leq k \leq r \\ 0 & r + 1 \leq k \leq n \end{cases} \quad . \qquad (B22)$$

From Eqs. (B6,B8),

$$W = \sum_{k=1}^{n} Q_k w_k' \quad . \qquad (B23)$$

Using the result of (B22) gives the desired expression:

$$W = \sum_{k=1}^{r} Q_k Q_k^t/(\lambda_k + \sigma_N^2) \quad P \quad . \qquad (B24)$$

Q E D

APPENDIX C

Proposition

Let S be a complex hermitian n x n matrix with eigenvalues λ_1, λ_2, ..., λ_n and corresponding eigenvectors $\underline{E_1}$, $\underline{E_2}$, ..., $\underline{E_n}$. Then a real symmetric matrix constructed as follows;

$$R = \left[\begin{array}{c|c} Re(S) & -Im(S) \\ \hline Im(S) & Re(S) \end{array}\right]$$

has following eigenvalues and eigenvectors

Eigenvalues λ_1, ..., λ_n, λ_1, ..., λ_n

$$\text{Eigenvectors} \quad _k = \left[\begin{array}{c} Re(E_k) \\ Im(E_k) \end{array}\right] \quad \text{for } k = 1, \ldots, n$$

$$_k = \left[\begin{array}{c} -Im(E_{k-n}) \\ Re(E_{k-n}) \end{array}\right] \quad \text{for } k = n+1, \ldots, 2n$$

Comments

1. Since S is hermitian (i) λ_j's are all real

    (ii) E_j's all complex

2. R is 2n x 2n symmetric matrix and as expected has real eigenvalues and eigenvectors.

Proof

R may alternatively be represented as

$$R = \frac{1}{2}\left[\begin{array}{c|c} s + \bar{s} & is_- + \overline{is} \\ \hline -is + \overline{-is} & s + \bar{s} \end{array}\right] \tag{C1a}$$

$$= \frac{1}{2}\left[\begin{array}{c|c} s & -is \\ \hline -is & s \end{array}\right] + \overline{\frac{1}{2}\left[\begin{array}{c|c} s & +is \\ \hline -is & s \end{array}\right]} \tag{C1b}$$

$$= \mathbf{\delta} + \bar{\mathbf{\delta}} \tag{C1c}$$

where

$$\mathbf{\delta} = \frac{1}{2}\left[\begin{array}{c|c} s & -is \\ \hline -is & s \end{array}\right] \quad . \tag{C2}$$

Consider the ℓth eigenvalue of S, λ_ℓ and the corresponding eigenvector E_ℓ. Construct a 2n dimensional vector

$$\mathbf{\delta}_\ell = \begin{bmatrix} E_\ell \\ -iE_\ell \end{bmatrix} \quad \text{for} \quad 1 \le \ell \le n \quad . \tag{C3}$$

The matrix product

$$\mathbf{\delta}\mathbf{\delta}_\ell = \frac{1}{2}\left[\begin{array}{c|c} s & -is \\ \hline -is & s \end{array}\right]\begin{bmatrix} E_\ell \\ -iE_\ell \end{bmatrix}$$

i.e.

$$\ell = \frac{1}{2}\left[\begin{array}{c} \underline{\quad SE_{\ell} + SE_{\ell} \quad} \\ -isE_{\ell} - isE_{\ell} \end{array}\right]$$

$$= \frac{1}{2}\left[\begin{array}{c} 2\lambda_{\ell}E_{\ell} \\ -2i\lambda_{\ell}E_{\ell} \end{array}\right]$$

$$= \lambda_{\ell}\left[\begin{array}{c} E_{\ell} \\ -iE_{\ell} \end{array}\right]$$

$$= \lambda_{\ell}\mathbf{\delta}_{\ell} \quad . \tag{C4}$$

Thus λ_{ℓ} is the ℓth eigenvalues and $\mathbf{\delta}_{\ell}$ is the ℓth eigenvector of $\mathbf{J}$ for $1 \leq \ell \leq n$. For $(n+1) \leq m \leq 2n$ we compute the eigenvalues and eigenvectors of   as follows.

For each m define $\ell = m-n$. Construct ϵ_m as

$$\mathbf{\delta}_m = \left[\begin{array}{c} iE_{\ell} \\ E_{\ell} \end{array}\right] = \left[\begin{array}{c} iE_{m-n} \\ E_{m-n} \end{array}\right] \quad \text{for} \quad n + 1 \leq m \leq 2n \quad . \tag{C5}$$

Proceeding as we did in (C4) we have

$$\mathbf{J}\mathbf{\delta}_m = \frac{1}{2}\left[\begin{array}{c|c} s & -is \\ \hline -is & s \end{array}\right]\left[\begin{array}{c} iE_{\ell} \\ E_{\ell} \end{array}\right]$$

$$= \frac{1}{2}\left[\begin{array}{c} \underline{iSE_{\ell} + iSE_{\ell}} \\ SE_{\ell} + SE_{\ell} \end{array}\right] = \frac{1}{2}\left[\begin{array}{c} i2\lambda_{\ell}E_{\ell} \\ 2\lambda_{\ell}E_{\ell} \end{array}\right] = \lambda_{\ell}\left[\begin{array}{c} iE_{\ell} \\ E_{\ell} \end{array}\right]$$

57

i.e.

$$\delta \delta_m = \lambda_\ell \delta_m = \lambda_m \delta_m \qquad \text{(C6)}$$

thus δ_m is the mth eigenvector with

$$\lambda_m = \lambda_\ell = \lambda_{m-n} \quad .$$

Since δ is hermitian;

$$\overline{\delta E_k} = \overline{\lambda_k E_k} ; \quad \overline{\delta E_k} = \lambda_k \overline{E}_k \quad .$$

Thus the eigenvalues of $\overline{\delta}$ are the eigenvalues of δ, and the eigen-vectors of $\overline{\delta}$ are the complex conjugates of the eigenvectors of .

Now construct

$$Q_k = \delta_k + \overline{\delta}_k \qquad \text{(C7)}$$

where

$$1 \le k \le 2n \quad .$$

Using the definition of R in (C1c), form the matrix product R_k.

$$RQ_k = (\delta + \overline{\delta})(\delta_k + \overline{\delta}_k)$$

$$= \delta \delta_k + \delta \overline{\delta}_k + \overline{\delta} \delta_k + \overline{\delta} \overline{\delta}_k$$

$$= \lambda_k \delta_k + \delta \overline{\delta}_k + \overline{\delta \overline{\delta}_k} + \lambda_k \overline{\delta} k$$

$$RQ_k = \lambda_k Q_k + \delta \overline{\delta}_k + \overline{\delta \overline{\delta}_k} \qquad \text{(C8)}$$

58

Now consider $\delta \overline{\delta}_k$ and substitute for δ from (C2) and $\overline{\delta}_k$ from (C3) or (C5) depending on value of k.

$\underline{1 \leq k \leq n}$

$$\delta \overline{\delta}_k = \frac{1}{2} \left[\begin{array}{c|c} S & iS \\ \hline -iS & S \end{array} \right] \overline{\left[\begin{array}{c} E_k \\ -iE_k \end{array} \right]}$$

$$= \frac{1}{2} \left[\begin{array}{c} S\overline{E}_k - S\overline{E}_k \\ -iS\overline{E}_k + iS\overline{E}_k \end{array} \right]$$

$$= 0 \qquad\qquad\qquad (C9a)$$

$\underline{n + 1 \leq k \leq 2n}$

$$\delta \overline{\delta}_k = \frac{1}{2} \left[\begin{array}{c|c} S & -iS \\ \hline -iS & S \end{array} \right] \overline{\left[\begin{array}{c} iE_{k-n} \\ E_{k-n} \end{array} \right]}$$

$$= \frac{1}{2} \left[\begin{array}{c} -iS\overline{E}_{k-n} + iS\overline{E}_{k-n} \\ -S\overline{E}_{k-n} + S\overline{E}_{k-n} \end{array} \right]$$

$$= 0 \quad . \qquad\qquad (C9b)$$

Substituting results of (C9a) and (C9b) in (C8) we have

$$RQ_k = \lambda_k Q_k \quad . \qquad\qquad (C10)$$

Thus λ_k is the eigenvalue of R and Q_k.

Eigenvalues λ_k and λ_{k+n} are equal, but the following argument shows that Q_k and Q_{k+n} are not linearly dependent.

Consider the equation

$$aQ_k + bQ_{k+n} = 0 \quad . \tag{C13}$$

If the only values (a,b) that satisfy (C13) are $(0,0)$, then Q_k and Q_{k+n} are linearly independent.

Using (C11) and (C12)

$$a \begin{bmatrix} Re(\delta_k) \\ \hline Im(\delta_k) \end{bmatrix} + b \begin{bmatrix} -Im(\delta_{k+n-n}) \\ \hline Re(\delta_{k+n-n}) \end{bmatrix} = 0$$

$$\begin{bmatrix} a & -b \\ b & a \end{bmatrix} \begin{bmatrix} Re(\delta_k) \\ \hline Im(\delta_k) \end{bmatrix} = 0$$

$$\begin{bmatrix} Re(\delta_k) & \vdots & -Im(\delta_k) \\ \hline Im(\delta_k) & \vdots & Re(\delta_k) \end{bmatrix} \begin{bmatrix} a \\ b \end{bmatrix} = 0 \quad .$$

Let

$$\begin{bmatrix} Re(\delta_k) & \vdots & -Im(\delta_k) \\ \hline Im(\delta_k) & \vdots & Re(\delta_k) \end{bmatrix} = \mathcal{J}$$

then

$$a = \frac{det \begin{bmatrix} 0 & \vdots & -Im(\delta_k) \\ \hline 0 & \vdots & Re(\delta_k) \end{bmatrix}}{det \; \mathcal{J}} = 0$$

and

$$b = \frac{\det\left[\begin{array}{c|c} \mathrm{Re}(\delta_k) & 0 \\ \hline \mathrm{Im}(\delta_k) & 0 \end{array}\right]}{\det \mathfrak{F}} = 0 \quad .$$

Therefore Q_k and Q_{k+n} are linearly independent.

APPENDIX D

Interpretation of the NED Plot for Small Jammer Separations

As was discussed in Section IV of this report, there is an apparent
conflict between the convergence rate indicated by the NED plot and the
convergence rate obtained in practice when the angular separation between
jammers becomes small. The values obtained from the NED plot are large,
showing that an extremely slow convergence mode exists. On the other
hand, intuition and experience indicate that two closely-spaced jammers
can be quickly eliminated using a single, broadened null. This appendix
examines these two viewpoints more closely and provides a resolution of
the apparent conflict.

In order to examine convergence rate in some detail, learning curves
were plotted for the three-element triangular array (Figure 4-3) using
several different jammer configurations. Figure D-1 is the learning
curve obtained with the strong jammer (Power = 100) at 40° and the weak
jammer (Power = 1) at 41°. For this 1^O jammer spacing, the error power
drops extremely rapidly to a value of less than 1×10^{-7}. This corresponds
to the rapid nulling that is intuitively expected from placing a single
notch on both signals. Once the rapid nulling has occurred, however,
the learning curve becomes essentially flat, and further reduction of
error power occurs at an extremely slow rate. This is the slow conver-
gence mode indicated by the large eigenvalue disparity. What is _not_
shown by the NED plot is the fact that, for the selected initial weights,
the slow mode becomes important only after error power has been reduced
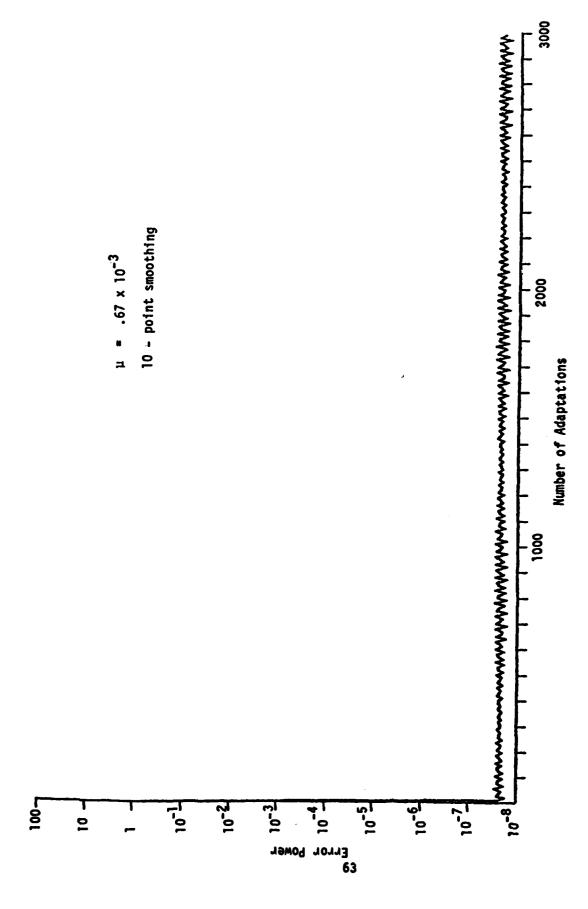to very low levels.

Figure D-1. Learning Curve for Three-Element Triangular Array with 1° Jammer Separation.

$\mu = .67 \times 10^{-3}$

10 - point smoothing

Number of Adaptations

Error Power

Learning curves for the same array configuration and jammer powers are shown in Figures D-2 and D-3 for the cases involving, respectively, 15° and 30° jammer separations. The 15° case is the same case that was treated in the body of this report. The NED is 12.5, and convergence occurs at about 26,100 adaptations. The 30° case has an associated NED of 3.5, and convergence occurs after some 9,800 adaptations. The error levels that are reached after the first few adaptation cycles differ by approximately an order of magnitude, with the error in the 15° case being the smaller of the two. In both cases, however, error levels after the initial rapid adaptation remain relatively high with respect to the arbitrarily selected convergence threshold of 1×10^{-6}. Convergence along the slow mode dominates in both cases, and the NED ratio comparison provides a rough measure of relative convergence rates:

$$\text{NED Ratio} = \frac{12.5}{3.5} = 3.57$$

$$\text{Ratio of Adaptation Times} = \frac{26,100}{9,800} = 2.70 \quad .$$

By making allowances for the differences in error levels after the first few adaptation cycles, the NED ratio between the 15° and 30° cases can be checked. Crossover of the two learning curves occurs at 3,340 adaptations. If times to convergence are compared from this point, the NED ratio is seen to accurately reflect comparative rates of convergence along the slow mode:

$$\text{Ratio of Adaptation Times} = \frac{26,100 - 3340}{9,800 - 3340} = \frac{22,760}{6,460} = 3.52 \quad .$$
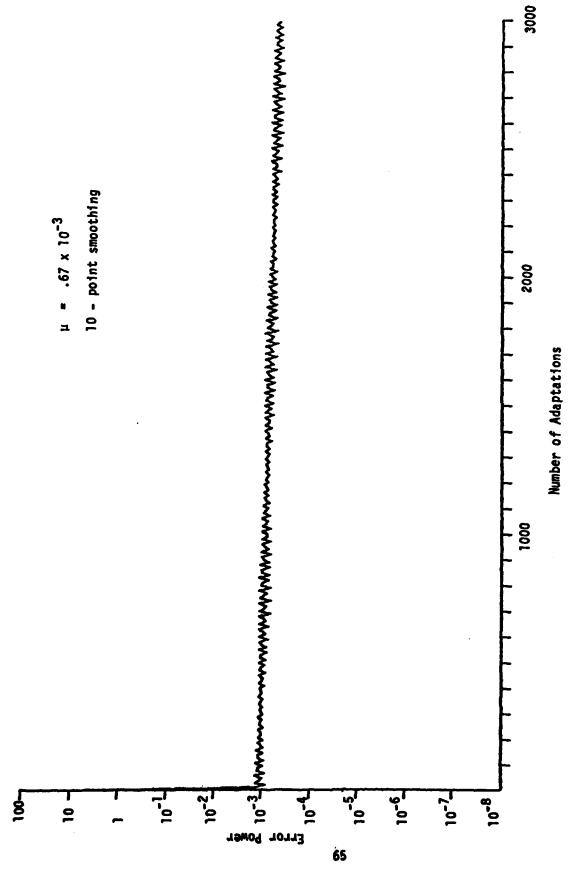
64

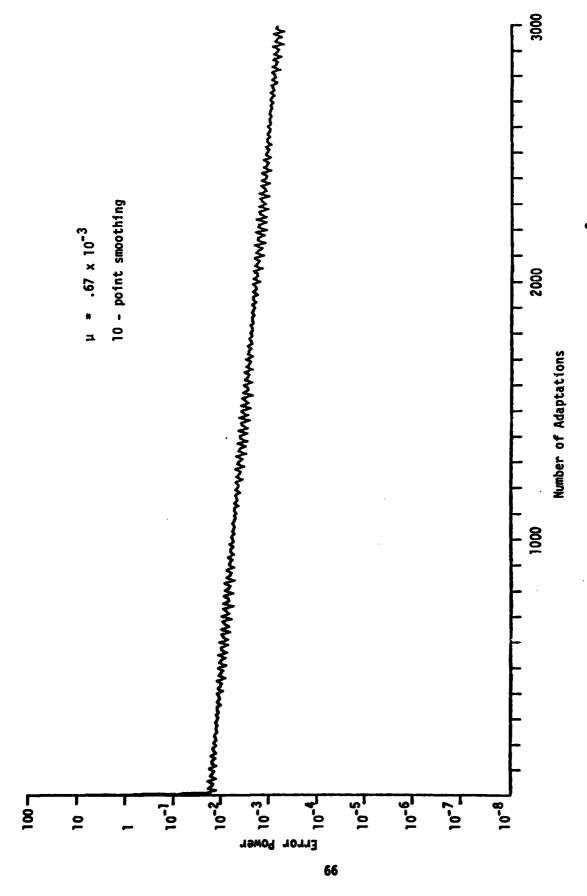Figure D-2.   Learning Curve for the Three-Element Triangular Array with 15° Jammer Separation.

65

Figure D-3. Learning Curve for the Three-Element Triangular Array with 30° Jammer Separation.

It can be seen that the NED provides a useful measure of convergence rate under the assumption that convergence occurs along the slow mode. In practice, however, convergence will typically occur along a mixture of modes, and the convergence time indicated by the NED will overbound the true time. Further work is needed to define the circumstances under which the estimate provided by the NED is useful and to provide more accurate convergence measures where the estimate is overly pessimistic. Consideration is being given to an exact solution for the two-jammer problem. This solution will involve calculating the optimal weights, determining the distance from the initial weights to the optimal weights, and decomposing this distance into components along the eigenvectors associated with the fast mode and the slow mode.

MISSION
of
Rome Air Development Center

RADC plans and executes research, development, test and selected acquisition programs in support of Command, Control Communications and Intelligence (C^3I) activities. Technical and engineering support within areas of technical competence is provided to ESD Program Offices (POs) and other ESD elements. The principal technical mission areas are communications, electromagnetic guidance and control, surveillance of ground and aerospace objects, intelligence data collection and handling, information system technology, ionospheric propagation, solid state sciences, microwave physics and electronic reliability, maintainability and compatibility.